THE JOURNAL OF PHYSICAL CHEMISTRY B

ARTICLE

pubs.acs.org/JPCB

Destabilization of Lipid Membranes by a Peptide Derived from Glycoprotein gp36 of Feline Immunodeficiency Virus: A Combined Molecular Dynamics/Experimental Study

Antonello Merlino,[†,‡] Giuseppe Vitiello,[†,§] Manuela Grimaldi,[∥] Filomena Sica,[†,‡] Elena Busi,[§,⊥] Riccardo Basosi,[§,⊥] Anna Maria D'Ursi,[∥] Giovanna Fragneto,[#] Luigi Paduano,[†,§] and Gerardino D'Errico*[,†,§]

[†]Department of Chemistry, University of Naples "Federico II", Complesso di Monte S. Angelo, Via Cinthia, I-80126 Naples, Italy

[‡]Istituto di Biostrutture e Bioimmagini, CNR, Naples, Italy

[§]CSGI (Consorzio per lo Sviluppo dei Sistemi a Grande Interfase), Florence, Italy

[∥]Department of Pharmaceutical Science, University of Salerno, Fisciano, Italy

[⊥]Department of Chemistry, University of Siena, Siena, Italy

[#]Institut Laue-Langevin, Grenoble, France

Supporting Information

ABSTRACT: Viral fusion glycoproteins present a membrane-proximal external region (MPER) which is usually rich in aromatic residues and exhibits a marked tendency to stably reside at the membrane interfaces, leading, through unknown mechanisms, to a destabilization of the bilayer structure. This step has been proposed to be fundamental for the fusion process between target membrane and viral envelope. In the present work, we investigate the interaction between an octapeptide (C8) deriving from the MPER domain of gp36 of feline immunodeficiency virus and POPC bilayers by combining experimental results obtained by neutron reflectivity, electron spin resonance, circular dichroism, and fluorescence spectroscopy with molecular dynamics simulations. Our data indicate that C8 binds to the lipid bilayer adsorbing onto the membrane surface without deep penetration. As a consequence of this interaction, the bilayer thickness decreases. The association of the peptide with the lipid membrane is driven by hydrogen bonds as well as hydrophobic interactions that the Trp side chains form with the lipid headgroups. Upon peptide—bilayer interaction, C8 forms transient secondary structures ranging from 3_{10} helices to turn conformations, while acyl chains of the peptide-exposed POPC molecules assume a more ordered packing. At the same time, lipid headgroups' hydration increases. The asymmetric lipid bilayer perturbation is proposed to play a fundamental role in favoring the membrane fusion process.

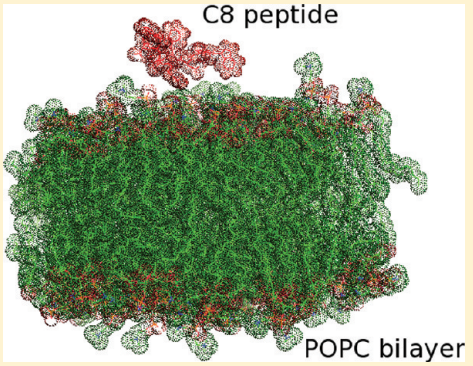

1. INTRODUCTION

Interactions between proteins/peptides and phospholipid bilayers are fundamental in a variety of key biological processes. Among these, membrane fusion is one of the most relevant, being involved in cell growth, subcellular compartmentalization, mitochondrial remodelling, hormone secretion, neurotransmission, and carcinogenesis.[1] Membrane fusion is also a rate-determining step in viral infection by "enveloped" viruses. These viruses, whose capsid is enclosed by a phospholipid bilayer, enter the target cell by fusion of their own envelope with the cell membrane. In this process, specific viral proteins, named fusion proteins, interacting with both viral and cellular membranes, facilitate their fusion.[2]

Viral fusion proteins deriving from different viruses (e.g., ebola, dengue, SARS, herpes simplex, and hepatitis C viruses) show a variety of molecular architecture. Furthermore, they usually act as homo- or heteromultimers. However, in all cases fusion is accomplished through a common mechanism of action, in which a large-scale protein conformational change is coupled to apposition and merging of the two bilayers.[3]

There is converging evidence that different domains of the viral fusion protein cooperate, playing different roles, in driving membrane fusion. A distinctly hydrophobic sequence, usually named fusion peptide, is deputed to enter the target cell membrane "anchoring" the virus on it. This is a necessary, but not sufficient, step for membrane fusion: even in the presence of a bridging protein, the two opposing membranes tend to preserve their integrity because of the high energy required for phospholipid rearrangement.[4] Other domains of the fusion protein are hypothesized to interact with the membranes lowering the energetic barrier thus allowing their final fusion. Particularly, the researchers' interest has focused on the

Received: May 23, 2011
Revised: November 18, 2011
Published: December 01, 2011

membrane-proximal external region (MPER), also named pre-transmembrane domain.[5]

Both the human immunodeficiency virus (HIV) and the feline analogue (FIV) effect cell entry via a mechanism that involves surface glycoproteins named gp41 and gp36, respectively.[6−8] These proteins present a tryptophan-rich MPER domain, whose action has been found to be crucial in the membrane fusion process.[9−12] However, the actual role played by this protein domain is still elusive.

We have recently investigated, through electron spin resonance (ESR) spectroscopy, the interactions between peptides derived from the gp36 MPER domain and phospholipid membranes. Initially, we considered a 20-mer peptide, named P59, corresponding to the ^{767}L-G^{786} sequence of gp36.[13] ESR experiments, using spin-labeled lipids, demonstrated that the P59 peptide associates with lipid bilayers. Analysis of these results, combined with the high-resolution nuclear magnetic resonance (NMR) investigation on P59 conformational preferences in micellar environments,[14] led us to hypothesize a key role, in stabilizing the peptide−bilayer interaction, played by the sequence extending from Trp^{770} to Ile^{777} (Trp-Glu-Asp-Trp-Val-Gly-Trp-Ile). To confirm our hypothesis, we successively investigated, by ESR, spectrofluorimetry and circular dichroism measurements, the interaction between an octapeptide, named C8, corresponding to the Trp^{770} to Ile^{777} sequence of gp36 and dimyristoylphosphatidylcholine liposomes (DMPC) bilayers,[15] finding that C8 adsorbs strongly on the bilayer surface. However, despite the large volume of experimental work, a clear conceptual framework for the mechanism of action of C8 on the bilayer microstructure is lacking.

In this work, we present a microstructural study on C8−palmitoyloleoylphosphatidylcholine (POPC) bilayers' interaction in which experimental results obtained by neutron reflectivity (NR), ESR, circular dichroism (CD), and spectrofluorimetry are combined with molecular dynamics (MD) simulations. POPC was chosen because it includes both a saturated (C16) and an unsaturated (C18) fatty acid like most of phospholipids present in mammalian cell membranes.[16] Furthermore, it has a well-established force field, which has been shown to reproduce experimental data in several MD studies.[17−23] The purpose of this work is to present a clear description at a molecular level of the effect of the C8−POPC interactions on the lipid bilayer microstructure to provide a high-resolution picture of the early events of the fusion process.

2. MATERIALS AND METHODS

2.1. Materials. The phospholipid palmitoyloleoylphosphatidylcholine (POPC) was obtained from Avanti Polar Lipids (Birmingham, AL). Spin-labeled phosphatidylcholines (*n*-PCSL) with the nitroxide group at different positions, *n*, in the *sn*-2 acyl chain, to be used for ESR experiments, were synthesized as described by Marsh and Watts.[24,25] The spin labels were stored at −20 °C in ethanol solutions at a concentration of 1 mg/mL.

Ultra-high-quality water (resistivity = 18.2 MΩ cm; Elga) was used in all experiments. D_2O for NR experiments was provided from the reactor at the Institut Laue-Langevin (ILL) in Grenoble, France. The solid supports for neutron reflection were 8 × 5 × 1 cm^3 silicon single crystals cut to provide a surface along the (111) plane. These were polished by Siltronix (Archamps, F) and cleaned for 15 min in a mixture of 1:4:5 $H_2O_2/H_2SO_4/H_2O$ at 80−85 °C, followed by ozonolysis.[26] This treatment leaves a natural oxide layer of 7−20 Å thickness and 3−5 Å roughness.

2.2. Peptide Synthesis. The amino acid sequence of C8 peptide is Ac-Trp-Glu-Asp-Trp-Val-Gly-Trp-Ile-CO-NH_2, and the deuterated C8-d_{5all} was synthesized including Trp-d_5 in all the Trp positions. Trp-d_5 including deuterons atoms on indole ring and NH-Fmoc protected group (L-tryptophan-*N*-Fmoc-(indole-d_5), 98%) was purchased from Cambridge Isotope Laboratories Inc. (Andover, MA).

C8 and C8-d_{5all} were synthesized on a manual batch synthesizer (PLS 4×4, Advanced ChemTech, Louisville, KY) using a Teflon reactor (10 mL), applying the Fmoc/tBu solid-phase peptide synthesis (SPPS) procedure. The Rink resin was swelled with *N*,*N*-dimethylformamide (DMF) (1 mL/100 mg of resin) for 3 h before use. Stepwise peptide assembly was performed by repeating for each added amino acid the following deprotection−coupling cycle. (1) Swelling: DMF (1 mL/100 mg of resin) for 5 min. (2) Fmoc deprotection: resin is washed twice with 20% piperidine in DMF (1 mL/100 mg of resin, one wash for 5 min followed by another wash for 20 min). (3) Resin washings: DMF (3−5 min). (4) Coupling: scale employing *O*-benzotriazole-*N*,*N*,*N*′,*N*′-tetramethyluronium hexafluorophosphate/*N*-hydroxybenzotriazole/*N*,*N*-diisopropylethylamine (DIPEA) (2.5:2.5:3.5 equiv) as the coupling system and 2.5 equiv of the Fmoc-protected amino acids. Each coupling was monitored by Kaiser test,[27] whose negative response indicated that recouplings were not needed. (5) Resin washings: DMF (3−5 min) and dichloromethane (1−5 min). After deprotection of the last NH-Fmoc group, peptides were acetylated with a solution of acetic anhydride (12.5%) and DIPEA (2.5%) in DMF for 2 h.

The protected hydrogenated peptide C8 was cleaved from the resin by treatment with trifluoroacetic acid (TFA)/H_2O/thioanisole (reagent K) (95:2.5:2.5 v/v). In contrast, to avoid D_2O/H_2O exchange, the protected peptide C8-d_{5all} was cleaved from resin by treatment with trifluoroacetic acid-*d* (TFA*d*)/D_2O/triisopropylsilane at a ratio of 10 mL to 0.5 g of resin at room temperature for 3 h.[28,29] TFA*d* (D, 99.5%) and deuterium oxide (D, 99.9%) (D_2O) were purchased from Cambridge Isotope Laboratories Inc. All the other reagents and solvents were purchased from Aldrich (St. Louis, MO) and were used as received.

After filtration of the exhausted resin, the solvent was concentrated in vacuo and the residue was triturated with ether. The crude peptide was purified by preparative reversed phase high performance liquid chromatography (HPLC) using a Jupiter (Phenomenex, Anzola Emilia (BO), Italy) C18 column (250−4.6 mm, 5 μm, 300 Å pore size). The column was perfused at a flow rate of 3 mL/min with a mobile phase containing solvent A (0.1% TFA in water). A linear gradient from 50% to 90% of solvent B (0.1% TFA in acetonitrile) for 40 min was adopted for peptide elution. The pure fraction was collected to yield a white powder after lyophilization. The molecular weight of the compound was determined by mass spectral analysis using a Finnigan LCQ-Deca ion trap instrument equipped with an electrospray source (LCQ Deca Finnigan, San Jose, CA). The samples were directly infused into the ESI source using a syringe pump set at a flow rate of 5 μL/min. Data were analyzed with Xcalibur software.

2.3. Sample Preparation. POPC liposomes, to be used for ESR, CD, and spectrofluorimetry experiments, were prepared by pouring appropriate amounts of phospholipid dissolved in dichloromethane/methanol (2/1 v/v) in small test tubes. For ESR experiments 1 wt %/wt of spin-labeled phosphatidylcholines in

ethanol was added. Dichloromethane, methanol, and ethanol, HPLC-grade solvents, were obtained from Merck (Darmstadt, Germany). A thin film of the lipid was produced by evaporating the solvent with dry nitrogen gas. Final traces of solvent were removed by subjecting the sample to vacuum desiccation for at least 3 h. The samples were then hydrated with 20−50 μL of 10 mM phosphate buffer, 137 mM NaCl, and 2.7 mM KCl, pH 7.4 (PBS) and vortexed, obtaining a suspension of multilamellar vesicles (MLVs). For ESR experiments, this suspension was transferred to a 25 μL glass capillary and flame-sealed. For CD and spectrofluorimetry experiments, large unilamellar vesicles (LUVs), obtained from MLVs by 9-fold extrusion through a polycarbonate membrane of 100 nm pore size, were preferred for their lower radiation scattering. Liposomal samples (both MLVs and LUVs) containing the peptide were prepared in a similar manner, except that the lipid film was hydrated directly with a peptide solution in PBS. For neutron reflectivity experiments, supported single lipid bilayers (SSLBs) were prepared by vesicles fusion:[30] small unilamellar vesicles (SUVs), of 25−35 nm in diameter, were formed by vortexing and sonicating for 3 × 10 min the MLVs suspension. The SUVs suspension (0.5 mg mL^{-1}) was injected into the NR cell, and allowed to diffuse and adsorb to the silicon surfaces over a period of 30 min. Afterward the sample cell was rinsed once with deuterated water to remove excess lipid. C8 solution was added after bilayer formation.

2.4. Neutron Reflectivity Measurements. Neutron reflectivity measurements were performed on the D17 reflectometer[31] at the high flux reactor of the Institut Laue-Langevin (ILL, Grenoble, France) in time-of-flight mode using a spread of wavelengths between 2 and 20 Å with two incoming angles of 0.8 and 3.2°.

In a neutron reflectivity experiment, the specular reflection at the silicon/water interface, R, is measured as a function of the wave vector transfer, q:

$$q = \frac{4\pi}{\lambda}\sin\theta \tag{1}$$

where λ is the wavelength and θ the angle of the incoming beam to the surface. $R(q)$ is related to the scattering length density across the interface, $\rho(z)$, by

$$R(q) = \frac{16\pi^2}{q^2}|\hat{\rho}(q)|^2 \tag{2}$$

where $\hat{\rho}(q)$ is the one-dimensional Fourier transform of $\rho(z)$:

$$\hat{\rho}(q) = \int_{-\infty}^{+\infty}\exp(-iqz)\rho(z)\,dz \tag{3}$$

$\rho(z)$ being a function of the distance perpendicular to the interface. ρ is related to the composition of the adsorbed species by

$$\rho(z) = \sum_j n_j(z)b_j \tag{4}$$

where $n_j(z)$ is the number of nuclei per unit volume and b_j is the scattering length of nucleus j.[32] The scattering lengths of the constituent fragments of any species adsorbed at the surface are the fundamental quantities from which the interfacial properties and microstructural information on the lipid bilayer are derived. Measurement of a sample in different solvent contrasts greatly enhances the sensivity of the technique.[33]

Samples were measured using H_2O, SMW (silicon-matched water), 4MW, and D_2O as solvent contrasts. SMW (ρ = 2.07 × 10^{-6} Å^{-2}) is a mixture of 38 vol % D_2O (ρ = 6.35 × 10^{-6} Å^{-2}) and 62 vol % H_2O (ρ = −0.56 × 10^{-6} Å^{-2}) with the same refraction index for neutrons as a bulk silicon, while 4MW (ρ = 4 × 10^{-6} Å^{-2}) consists of 66 vol % D_2O and 34 vol % H_2O.

Neutron reflectivity profiles were analyzed by box model fitting using the Afit program.[34] It allows the simultaneous analysis of reflectivity profiles from the same sample in different water contrasts, characterizing each layer by its thickness, ρ, solvent volume fraction, and interfacial roughness. These parameters are varied until the optimum fit to the data is found. Although more than one model can be found for a given experimental curve, the number of possible models is greatly reduced by a prior knowledge of the system, which allows defining upper and lower limits of the parameters to be optimized, by the elimination of the physically meaningless parameters, and most importantly by the use of different isotopic contrasts.[33] Initially, the bare silicon substrate was characterized in terms of thickness and roughness. The set of NR profiles were calculated for a uniform single layer model (the silicon oxide layer) of thickness 8 ± 1 Å, roughness 9 ± 1 Å, and a scattering length density of 3.41 × 10^{-6} Å^{-2}, corresponding to 100% SiO_2. This step was followed by the characterization of the lipid bilayer and finally of the C8-interacting bilayer. The peptide was added to the bilayer by injecting in the cell an aqueous solution (0.25 mg mL^{-1}) in order to obtain a 0.5:1 peptide/lipid weight ratio.

2.5. ESR Spectroscopy. ESR spectra of lipid and lipid/peptide samples were recorded with a 9 GHz Bruker Elexys E-500 spectrometer (Bruker, Rheinstetten, Germany). Samples prepared for ESR measurements contained POPC (10 mg mL^{-1} corresponding to 1.3 × 10^{-2} M) and C8 at 0.5:1 weight ratio (corresponding to 0.33 molar ratio). Such a high ratio was chosen to be sure of the lipid bilayer saturation condition.[15] Capillaries containing the samples were placed in a standard 4 mm quartz sample tube containing light silicone oil for thermal stability. The temperature of the sample was regulated at 37 °C and maintained constant during the measurement by blowing thermostated nitrogen gas through a quartz Dewar. The instrumental settings were as follows: sweep width, 120 G; resolution, 1024 points; modulation frequency, 100 kHz; modulation amplitude, 1.0 G; time constant, 20.5 ms, incident power, 5.0 mW. Several scans, typically 16, were accumulated to improve the signal-to-noise ratio. Values of the outer hyperfine splitting, $2A_{max}$, were determined by measuring, through a homemade MATLAB-based routine, the difference between the low-field maximum and the high-field minimum.[35,36] The main source of error on the $2A_{max}$ value is the uncertainty in composition of samples prepared by mixing few microliters of mother solutions. For this reason, reproducibility of $2A_{max}$ determination was estimated by evaluating its value for selected independently prepared samples with the same nominal composition. It was found to be ±0.4 G. Simulations of some ESR spectra were performed using a program based on the stochastic Liouville equation[37] further modified in our laboratory[38,39] equipped with a Simplex least-squares best-fit algorithm.

2.6. Circular Dichroism Spectroscopy. CD experiments were performed at 37 °C on a 810-Jasco spectropolarimeter, using a quartz cuvette with a path length of 1 mm. CD spectra of C8 were measured in PBS and in the presence of POPC unilamellar vesicles. The spectra are an average of three consecutive scans from 250 to 200 nm, recorded with a bandwidth of 2.0 nm, a time constant of 16 s, and a scan rate of 5 nm min^{-1}. Mean residues ellipticities, $[\theta]$, were calculated as (MRW × θ)/(10 × d × c). MRW = $M/(n-1)$, where M is the molecular mass

of the peptide and n is the number of amino acids ($n - 1$ is the number peptide bonds). θ is the observed ellipticity in degrees, d is the path length in centimeters, and c is the concentration in g mL^{-1}. Samples prepared for CD measurements contained the peptide (1×10^{-4} M) and the phospholipid at a 10-fold higher concentration (1×10^{-3} M). During all the measurements, the trace of the high tension voltage was checked to be less than 700 V, which should ensure reliability of the data obtained.[40] Base lines of either solvent or vesicular suspensions without peptide were subtracted from each respective sample to yield the peptide contribution.

The propensity of the peptide to assume a helical conformation was estimated from measurements of mean residue ellipticity at 222 nm.[41] We used $[\theta]_{222}$ values of 0 and $-40\,000$ $(1 - 2.5/n)$ deg cm^2 dmol^{-1} per amino acid residue for 0% and 100% helicity. The correction for aromatic CD contributions to $[\theta]_{222}$ due to two internal Trp residues was applied ($[\theta]_{222}^{\text{aromatic}} = -2.300$ per residue). Finally, the fraction of helix was calculated as $[\theta]_{222}/([\theta]_{222}^{\text{helix}} + [\theta]_{222}^{\text{aromatic}})$.

2.7. Fluorescence Titration Measurements. C8−phospholipid interactions were also studied by monitoring the changes in the Trp fluorescence emission spectra of the peptide upon addition of increasing amounts of POPC unilamellar vescicles. Fluorescence measurements were performed at 37 °C using a Jasco FP750 spectrofluorimeter equipped with a thermostatically controlled cuvette holder. The excitation wavelength was 280 nm and emission spectra were recorded between 310 and 450 nm, with slit widths of 2 nm.

The titration was performed by adding measured amounts of a solution containing the peptide (1×10^{-4} M) and suspended lipid vesicles to a weighed amount of a solution of the peptide at the same concentration, initially put into the spectrofluorimetric cuvette. In this way, the lipid concentration was progressively increased (from 0 to $\sim 1 \times 10^{-3}$ M), while the peptide concentration remained constant during the whole titration. After each addition there was a 20 min wait to ensure equilibrium had been reached.

The change in the peptide fluorescence has been reported by Christiaens et al.[42] to follow the relation:

$$F = \frac{(F_0[\mathrm{P_F}] + F_1[\mathrm{PL}])}{([\mathrm{P_F}] + [\mathrm{PL}])} \tag{5}$$

where F is the fluorescence intensity at a given added lipid concentration. F_0 and $[\mathrm{P_F}]$ are the fluorescence intensity and concentration of the unbound peptide, respectively, while F_1 and $[\mathrm{PL}]$ are the fluorescence intensity and concentration of the peptide−lipid complex. $[\mathrm{PL}]$ can be obtained via the definition of the dissociation (association) constant:

$$K_\mathrm{d} = \frac{1}{K_\mathrm{a}} = \frac{([\mathrm{P_F}][\mathrm{L_F}])}{[\mathrm{PL}]} \tag{6}$$

with K_d dissociation constant, K_a association constant, and $[\mathrm{L_F}]$ free lipid concentration.

Equation 6 can be rearranged to the following quadratic equation:

$$[\mathrm{PL}]^2 - [\mathrm{PL}]\left([\mathrm{P_{tot}}] + \frac{[\mathrm{L_{tot}}]}{n} + K'_\mathrm{d}\right) + \frac{[\mathrm{L_{tot}}]}{n}[\mathrm{P_{tot}}] = 0 \tag{7}$$

The parameter n, representing the formal number of phospholipid molecules that are involved in a binding site for one peptide, is introduced in order to account for the formal stoichiometry of binding ($K'_\mathrm{d} = K_\mathrm{d}/n$). The solution of this quadratic equation is thus given by

$$[\mathrm{PL}] = \frac{\left\{S \pm \left(S^2 - 4\left(\frac{[\mathrm{L_{tot}}]}{n}\right)\right)[\mathrm{P_{tot}}]^{1/2}\right\}}{2} \tag{8}$$

with

$$S = [\mathrm{P_{tot}}] + \frac{[\mathrm{L_{tot}}]}{n} + K'_\mathrm{d}$$

Substitution of eq 8 into eq 5 yields an equation of F as a function of $[P_{tot}]$ and $[L_{tot}]$. By plotting the measured fluorescence intensity as a function of $[L_{tot}]$, K'_d and n can be determined through a nonlinear best-fitting procedure of the experimental fluorescence intensities at a fixed wavelength. K_d is obtained by multiplying K'_d by n.

2.8. Molecular Dynamics. All the computer simulations reported in this study were performed using GROMACS 3.2 package[43] and the GROMOS96 force field. In the C8−POPC binding simulations, the starting model of C8 obtained by NMR measurements, performed in membrane-mimicking DMSO/water mixtures,[44] was placed in a box containing a mixture of POPC lipids and water molecules. After the peptide insertion in the box, all water molecules with oxygen atoms closer to 0.40 nm from a non-hydrogen atom of the peptide were removed. Initially, the peptide is solvated in the water phase at a distance of 7 Å from the lipid bilayer. Three simulations have been performed with different initial C8 positions. The simulation time of the three trajectories is 70 ns. The only difference between these simulations is in the equilibration process: to equilibrate the systems, five simulations of 10 ps were performed in one case, six in the second case, and eight in the last case. In the equilibration process the atomic coordinates of the peptide were restrained to the initial positions. This resulted in final systems containing 128 lipids, the C8 molecule, and about 10 950 water molecules. Since the analysis of the three simulations showed similar results, only the features of one of the three trajectories are described.

For the simulations of C8 in solution, the peptide was solvated in a cubic box containing 3654 water molecules. Two starting structures were chosen for these simulations: the NMR model and a random structure. The simulation time of these trajectories is 70 ns. Molecular dynamics simulations have been performed using the procedure described elsewhere.[45−47] Briefly, the temperature was set to 310 K by weakly (τ = 0.1 ps) coupling the system to an external bath.[48] Likewise, the pressure was kept constant by weakly (τ = 0.1 ps) coupling the system to a pressure bath of 1 bar. Bond lengths were constrained by the linear constraint solver (LINCS) algorithm, allowing a time step of 2 fs.[49] Particle mesh Ewald method (PME)[50] was used for the treatment of electrostatic interactions for atoms at a distance greater than 9 Å. Short-range repulsive together with attractive dispersion interactions were described by a Lennard-Jones potential, which was cut off at 10 Å. The force field and the coordinates for POPC were downloaded from the Tieleman group Web site (http://mouse.bio.ucalgary.ca) and are the same as used for other works performed by us[19,20] and other authors.[21−23]

The lipid bilayer has been characterized by the analysis of membrane thickness, defined as the average phosphate−phosphate distance and of the density profile. Lipid tail parameters have

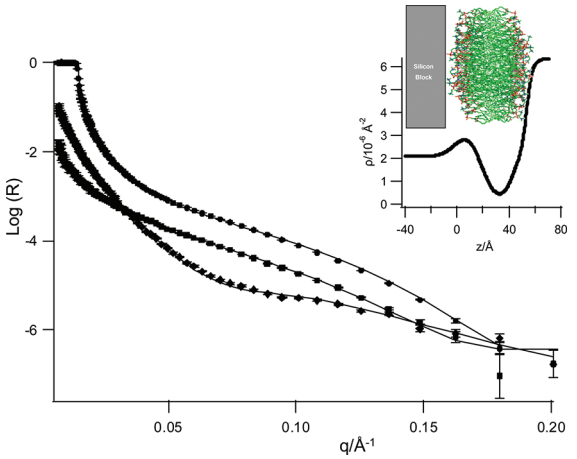

Figure 1. Neutron reflectivity profiles (points) and best fits (continuous lines) corresponding to pure POPC bilayer in (●) D_2O, (■) SMW, and (♦) H_2O solvents. The inset shows the ρ profile for the POPC bilayer in D_2O and a system snapshot obtained by MD simulations.

been calculated with respect to the membrane normal axis. The helicity of the peptide has been determined by dictionary of secondary structure of proteins (DSSP).[51] Images have been created with PyMOL (www.pymol.org).

3. RESULTS

3.1. Neutron Reflectivity Measurements. The pure POPC bilayer was characterized using D_2O, SMW, and H_2O as isotopic contrast solvents. The curves are shown in Figure 1, and the parameters used to fit the curves simultaneously from all the contrasts are given in Table 1. A five-box model was found to best fit the data. The first two correspond to the silicon block and to the thin solvent layer interposed between the silicon surface and the adsorbed bilayer. The three other boxes describe the lipid bilayer, which is subdivided in the inner headgroups, the hydrophobic chains, and the outer headgroups layers. The theoretical ρ of the lipid headgroups, calculated through eq 4, is equal to 1.86×10^{-6} Å^{-2}, while the ρ of acyl chains is equal to -0.29×10^{-6} Å^{-2}.[52] These values were kept constant during the data analysis, since their optimization was found to give no fitting improvement. Thus, the parameters obtained from the best-fit procedure are the thickness and the roughness of each box plus the solvent content expressed as volume percent. Inspection of Table 1 shows that the overall thickness of the bilayer is 44 ± 1 Å, while the roughness of all the boxes is the same as for the bare block.

The effect of the presence of C8 peptide in the bilayer was studied by measuring the neutron reflectivity curves of the fully hydrogenated POPC to which the peptide with deuterated Trp residues was added. Four contrast solvents, D_2O, 4MW, SMW, and H_2O, were used and NR curves are shown in Figure 2. Data from peptide-interacting bilayer were fitted by an additional layer with respect to the case of pure POPC model. This layer prominently consists of the peptide molecules interacting with the outer bilayer surface; its ρ, calculated by eq 4, is equal to 3.66×10^{-6} Å^{-2}. In Table 2, all values of molecular properties of both phospholipid and peptide are reported. Interestingly, in order to obtain a good curves fitting, the ρ of the chains region was changed from -0.29×10^{-6} to -0.20×10^{-6} Å^{-2} and, for the external headgroups leaflet, from 1.86×10^{-6} to 2.10×10^{-6} Å^{-2}. This indicates that the presence of the peptide effectively perturbs the outer hydrophilic layer of the POPC membrane and that this perturbation propagates in the chain region.

Table 1. Parameters Derived from Model Fitting the Reflectivity Profiles for (a) the Pure POPC and (b) after C8 Addition

interfacial layer	thickness (Å)	% solvent	roughness (Å)
	(a) Pure POPC		
water	3 ± 1	100	8 ± 1
inner headgroups	8 ± 1	31 ± 10	9 ± 1
chains region	28 ± 1	–	11 ± 1
outer headgroups	8 ± 1	33 ± 10	8 ± 1
	(b) After C8 Addition		
water	3 ± 1	100	8 ± 1
inner headgroups	6 ± 1	52 ± 10	9 ± 1
chains region	31 ± 1	–	11 ± 1
outer headgroups	5 ± 1	66 ± 10	9 ± 1
interacting peptide	5 ± 1	54 ± 10	8 ± 1

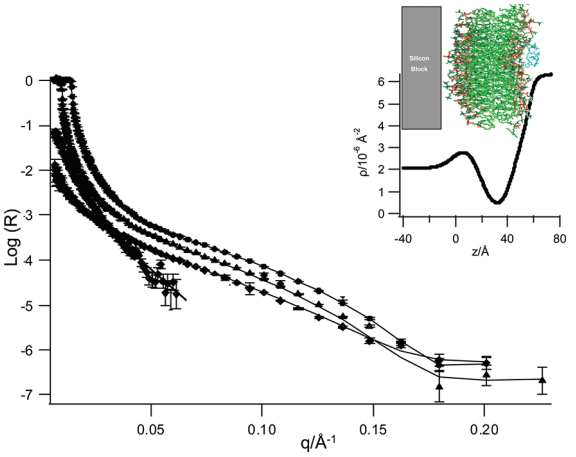

Figure 2. Neutron reflectivity profiles (points) and best fits (continuous lines) corresponding to POPC bilayer with C8 peptide in (●) D_2O, (▲) 4MW, (■) SMW, and (◆) H_2O solvents. In the last set, data at high q fall quickly into the background due to the roughness of the layer and incoherent scattering of the solvent. The inset shows the ρ profile for the bilayer in D_2O after peptide addition and a system snapshot obtained by MD simulations.

Table 2. Molecular Properties of POPC Phospholipid and C8 Peptide

	POPC	C8 peptide
$V_{headgroup}$ (Å^3)	322.1	
$\rho_{headgroup}$ ($\times 10^{-6}$ Å^{-2})	1.86	
V_{chains} (Å^3)	933.7	
ρ_{chains} ($\times 10^{-6}$ Å^{-2})	−0.29	
V_{mol} (Å^3)		1410.3[a]
M (g mol^{-1})		1129
ρ ($\times 10^{-6}$ Å^{-2})		3.66

[a] Peptide molecular volume is calculated from amino acid volume data reported from Zamyatin.[72]

dx.doi.org/10.1021/jp204781a |J. Phys. Chem. B 2012, 116, 401–412

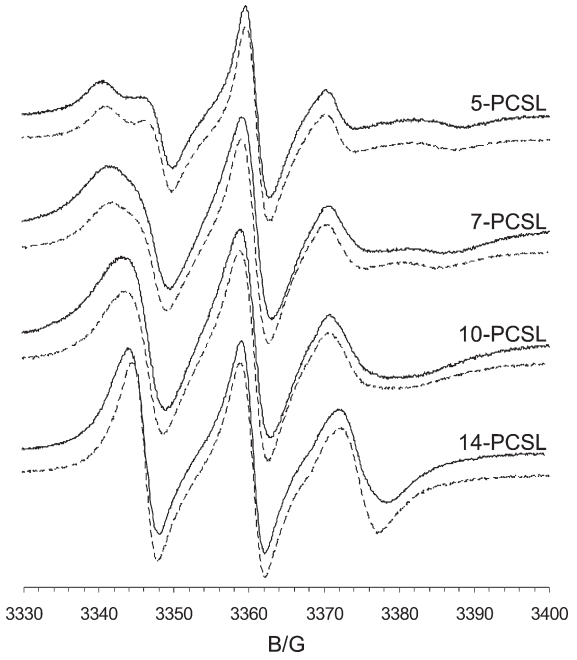

Figure 3. ESR spectra of *n*-PCSL positional isomers of spin-labeled phosphatidylcholine in fluid-phase palmitoyloleoylphosphatidylcholine bilayer membranes, in the presence (solid line) and in the absence (dashed line) of 0.5:1 wt/wt C8 at 37 °C.

The values of all parameters optimized in curves fitting are reported in Table 1. Please note that a model without the water layer between the substrate and the bilayer gave a worse fit to the data. No changes in the roughness of the bilayer occurred upon the introduction of peptide. In contrast, the thickness and the solvent content of the various boxes are different with respect to the pure POPC bilayer. The thickness values of both layers corresponding to the polar headgroups slightly decrease while the thickness of the chains region increases. The total thickness of the bilayer decreases by ∼2 Å. The more evident variations are observed for the solvent content values of both inner and outer headgroups layers that dramatically increase, even though to a different extent. While in the case of the outer hydrophilic headgroups layer this increase is directly related to the peptide binding, the changes in the inner headgroups layer indicate that the peptide effectively perturbs the whole bilayer structure. The lower extent of perturbation of the inner leaflet with respect to the outer one originates an asymmetry in the bilayer structure.

3.2. Spectroscopic Analysis. ESR spectroscopy by use of spin-labeled substances (peptides and/or lipids) has been proved to give substantial information on the interaction between viral fusion peptides and lipid membranes.[13,15,53−56] Association of these peptides with lipid membranes can be detected from the perturbation of the chain mobility of spin-labeled lipids, as reported in the literature for membrane proteins.[57]

In the present work, perturbation caused by C8 binding to POPC bilayers is investigated by analyzing changes in the ESR spectra of spin-labeled lipids included in the membrane. Four phosphatidylcholines spin-labeled at different positions in the *sn*-2 chain, *n*-PCSL (n = 5, 7, 10, 14), were employed, with the aim to monitor the changes in structuring and dynamics of the hydrophobic inner region of the bilayer. Figure 3 shows the *n*-PCSL ESR spectra in the presence and absence of C8 at a peptide to lipid ratio of 0.5:1 wt/wt. In the presence of C8, slight but significant perturbations in the spectra of all spin-labeled lipids are found.

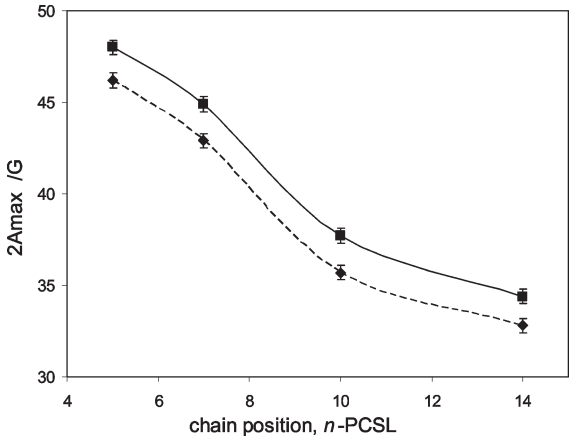

Figure 4. Dependence on spin-label position, *n*, of the outer hyperfine splitting, $2A_{max}$, of *n*-PCSL in membranes of POPC, in the absence (dashed line, solid diamonds) and in the presence of 0.5:1 wt/wt C8 (continuous line, solid squares). T = 37 °C. Lines are guides for the eyes.

In an attempt to quantitatively describe this behavior, we evaluated the outer hyperfine splitting, $2A_{max}$, which is a reliable and easy-to-perform estimate of the segmental chain mobility. $2A_{max}$ is defined as separation, expressed in gauss, between the low-field maximum and the high-field minimum, and tends to increase with increasing the restriction in local chain mobility. Figure 4 shows the dependence of the outer hyperfine splitting, $2A_{max}$, on chain position, *n*, for the *n*-PCSL spin labels in fluid POPC membranes, with and without a saturating amount of peptide. In both cases, $2A_{max}$ decreases with increasing *n*. In the presence of C8 the characteristic flexibility gradient with chain position of the fluid lipid bilayer membranes is preserved, but $2A_{max}$ is increased at all spin-label positions by roughly the same extent (≈2 G). Particularly, for what concerns the spin label presenting the nitroxide in a deeper position, 14-PCSL, there is no appearance of a second component in the spectra, corresponding to spin-labeled lipid chains whose motion is restricted. This is evidence that the peptide binds solely at the membrane surface and does not penetrate appreciably into the membrane interior, as does, for instance, the HIV fusion peptide gp41-FP.[53] Thus, in the case of C8, ESR results indicate that perturbations induced by surface association of the peptide propagate throughout the lipid chains, resulting in a reduction of the segmental mobility of the methylene groups with $n \geq 5$. In order to ensure that variations in the spectra line shape is determined by changes in segmental acyl chain mobility and not in magnetic parameters, simulations of 5-PCSL and 14-PCSL spectra, in the absence and in the presence of C8, were performed (see Figures S1 and S2 in the Supporting Information). Results show that, while magnetic parameters remain unchanged, the perpendicular components of the diffusion anisotropic tensor vary, giving the reorientational times τ_c reported in Table S1 in the Supporting Information. The τ_c trends are consistent with the $2A_{max}$ trends discussed above.

Peptide positioning relative to POPC bilayer was further investigated by intrinsic Trp fluorescence emission measurements. The Trp emission spectra of C8 peptide measured either in buffer or in the presence of increasing amounts of lipid vesicles are shown in Figure 5. C8 in water gives a Trp emission spectrum typical of an aqueous environment (λ_{max} = 354 nm), indicating

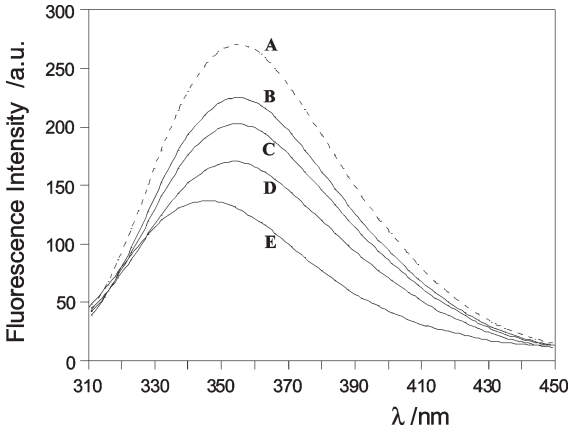

Figure 5. Fluorescence emission spectra of C8 peptide in aqueous phosphate buffer (A, dashed line), and in POPC unilamellar liposomes (solid line) at different lipid concentrations: B, 0.16 mM; C, 0.39 mM; D, 0.6 mM; and E, 0.92 mM. T = 37 °C.

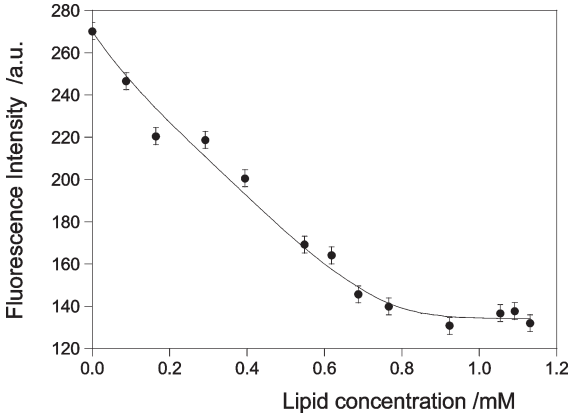

Figure 6. Fluorescence titration curve of C8 peptide with phospholipid liposomes at T = 37 °C.

that the Trp side chains are exposed to the aqueous medium. The presence of POPC liposomes causes a slight blue shift of the emission maximum to shorter wavelength (λ_{max} = 347 nm) and a reduction of the fluorescence quantum yield. No shoulder at lower wavelength appears. The limited extent of the shift indicates that the Trps are greatly exposed to the solvent.[58] These results indicate that, despite the interaction between C8 and POPC liposomes, all the Trp residues of this peptide are not significantly inserted in the apolar inner core of the bilayer. The C8 fluorescence intensities at 354 nm are plotted as a function of the lipid concentration in Figure 6. Fitting these data to the equation reported in the Materials and Methods section allows to evaluate the apparent peptide−lipid association constant, K_a, and the number of phospholipid molecules, n, required to bind a peptide. It was obtained $K_a = (8.3 \pm 0.6) \times 10^5\ M^{-1}$ and $n = 6 \pm 2$, respectively.

The conformational preferences of C8 in the presence of POPC liposomes were investigated by means of CD spectroscopy. The peptide in buffer presents a spectrum with the typical shape of a random coil structure, including a negative band at 202 nm. In the presence of POPC liposomes the spectrum assumes the double-well shape typical of a turn−helical structure, including negative bands at 205 and 216 nm (Figure 7).

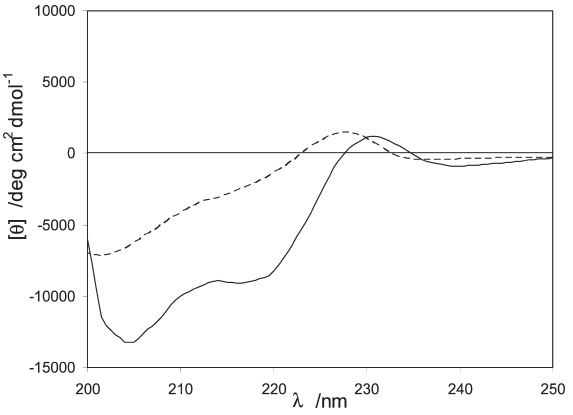

Figure 7. C8 CD spectra in aqueous phosphate buffer (dashed line), and in POPC unilamellar liposomes (solid line). T = 37 °C.

From $[\theta]_{222}$ the helix content has been estimated to be ∼20%. In the case of a short peptide like C8, this value has to be regarded as a time-averaged propensity to assume turn−helical structures.

3.3. MD Simulations. We have first analyzed MD simulations of C8 peptide in solution. These simulations were used as a test of the protein force field to determine whether MD data are in agreement with those obtained experimentally and to exclude possible artifacts induced by the force field choice, particularly the formation of β-hairpin structures that are known to be favored when GROMOS96 is used.[59] In our simulations, initial peptide conformation was set to that obtained by NMR measurements performed in DMSO/water mixed solvent.[44] This NMR structure, depicted in Figure S3A in the Supporting Information, indicates a strong C8 propensity to assume a turn−helical conformation in membrane-mimicking environments. A 70 ns simulation of C8 in aqueous solution showed that the peptide had very little propensity to form α-helical structure in water. In fact, as can be seen from Figure S3B which shows the number of structured residues (in α-helix, bend and turns) as a function of time, the initial model rapidly unfolds and the structure was not fully recovered during the rest of the simulation. Similarly, starting from a random model, no significant formation of α-helical structure was observed during an additional 70 ns simulation (Figure S3C). These results are consistent with CD data suggesting that C8 is unstructured in solution.

In the study of C8 interactions with POPC bilayer, three initial positions of the NMR structure[44] obtained in membrane-mimicking environment were chosen to eliminate any bias due to the starting configuration. In all cases, the minimum distance between the peptide and the bilayer is 0.7 nm. C8 was attracted to the surface of the bilayer in all simulations, independent of the starting position. The peptide comes into close contact with the bilayer headgroups within the first nanosecond and equilibrates at the surface for the remainder of the simulation (up to 70 ns) (Figure S4 in the Supporting Information). The secondary structure of the peptide drastically changes throughout the simulations. The peptide loses most of its starting secondary structure to become a random coil within the first nanosecond and subsequently it only transiently folds as a 3_{10} helix with turn structures (Figure S5 in the Supporting Information), substantially agreeing with the NMR experimental results. At the bilayer−water interface, the structure was maintained throughout with 2−4 residues of the peptide assuming helical and turn structures randomly sampled. In the path taken for binding,

dx.doi.org/10.1021/jp204781a |J. Phys. Chem. B 2012, 116, 401–412

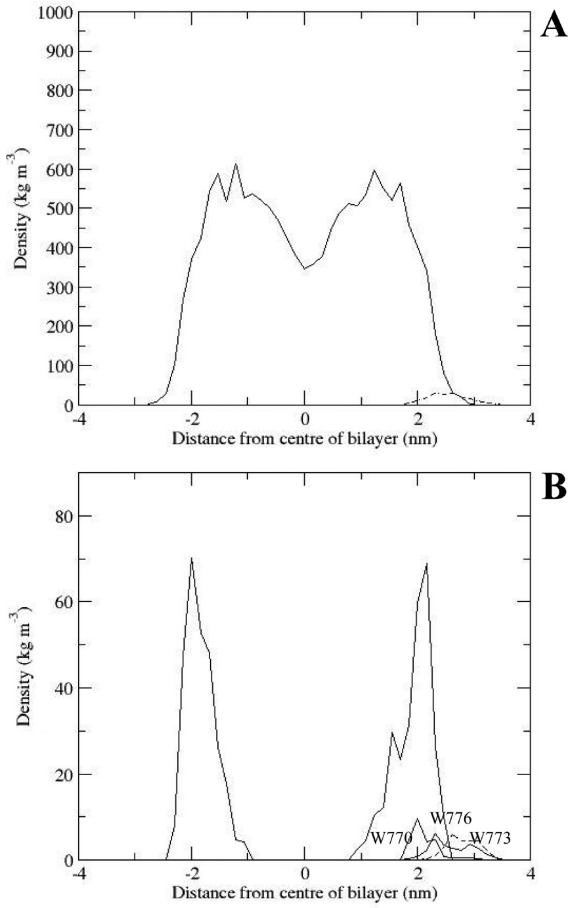

Figure 8. Density profile of (A) the POPC bilayer (solid lines) and of the C8 peptide (dashed lines); (B) phosphorus atoms (solid line) and Trp residues (black line for Trp770, gray line for Trp776, and dashed line for Trp773).

C8 peptide approaches the POPC bilayer surface without making significant contacts. Upon binding to membrane, strong interactions are observed between the peptide and the headgroups of the phospholipids.

The molecular density profile and the distribution of selected atoms or chemical groups of the bilayer along the axis perpendicular to the membrane surface in the presence and in the absence of the peptide are reported in Figure 8 and Figure S6 in the Supporting Information. Results are plotted relative to the center of the bilayer along the bilayer normal (z-axis). In particular, in Figure 8A the densities of the peptide and of the bilayer are shown, whereas in Figure 8B the density of Trp residues is compared with that of phosphorus atoms. The data in Figure 8A, B clearly show that the C8 is bound to the bilayer reaching the headgroup region and that the Trp residues are arranged so that they are facing toward the interior of the bilayer. Trp770 (numbering scheme of gp36) appears to be located farthest inside the POPC bilayer, while the other two Trp are anchored between the phosphate head groups and bulk water, i.e., at the water−membrane interface. The minimum distance between the Trp side chains and the POPC molecules as a function of time (Figure S7 in the Supporting Information) reveals that at least two of the three Trp (Trp770 and Trp776) are continuously bound to the membrane during the simulation. A model displaying the location of C8 on the bilayer surface, together with representative interactions with lipid molecules, is shown in Figure 9. The peptide orients such that the side chains of Trp770 and 776 form hydrogen bonds as well as hydrophobic interactions with the lipids, and the charged Glu and Asp residues (Glu771 and Asp772) remain hydrogen bonded with the oxygens of the lipid headgroups. Indoles of the Trp residues present the plane either parallel to the lipid chains or at an oblique angle to the membrane normal (Figure 9B,C). No conserved hydrogen bonds between the peptide backbone and the headgroups of the lipid bilayer are found.

In total, during the simulations, C8 is in contact with atoms belonging to 24−30 different POPC molecules, although, typically, the peptide binds 8−10 POPC molecules simultaneously. Peptide binding induces a decrease of 0.5−1 nm^2 of solvent-accessible surface for POPC oxygen and nitrogen atoms, which is likely to be due to their involvement in the lipid−peptide H-bonding. At the same time, MD results indicate an increase of 2−4 nm^2 of the solvent-accessible surface for POPC carbon atoms. This last result has to be interpreted as an increase of exposure to the solvent of the carbon atoms present in the lipid headgroup (i.e., those of glycerol and choline group). A snapshot showing water molecules in the lipid headgroup region is reported in Figure 9E. Water molecules form a network of hydrogen bonds with the oxygen atoms of glycerol and choline groups and hydrate carbon atoms. No water molecules are found in the acyl chain region. Thus, the lipids perturbation due to peptide interaction allows a better hydration of the exposed headgroups. POPC bilayer thickness, with and without the presence of C8, is reported in Table 3. By comparison of these values, it can be concluded that the C8 binding provokes a thinning effect of 3−5 Å. The reduction of the bilayer thickness induced by the peptide is confirmed by visual inspection of the trajectories and also suggested by Figure 9A, where the formation of a hollow on the bilayer surface can be detected. Notably, as can seen in Figure 9A, the C8-binding induced perturbations are localized, provoking a local thinning of the membrane, mainly of the lipid leaflet exposed to the peptide.

Figure S6 in the Supporting Information indicates that the overall density distribution of the different membrane component is similar in the presence and in the absence of the peptide, although a slight increase of the lipid headgroup density is observed when the peptide is in contact with the membrane.

MD simulations also show that peptide binding to the bilayer surface reflects in the microstructuring and dynamics of the lipid molecules. The calculated order parameters of the lipids in direct contact with the peptide compared with those of the other lipids constituting the bilayer are reported in Figure 10A. For POPC molecules in contact with C8, calculated values are slightly higher in magnitude (indicating more order in the system), particularly for the last atoms of the chain ($n \geq 8$). Similar results have been obtained comparing the root-mean-square fluctuations of POPC molecules in the presence and in the absence of the peptide. Interestingly, a slightly different effect of peptide binding on the two monolayers is also observed. In fact, inspection of Figure 10B shows that, in the peptide-bound leaflet, acyl chain mobility is slightly higher close to the interface (n = 2, 3) and somewhat lower in the more internal region ($n \geq 7$).

4. DISCUSSION

C8 is an octapeptide deriving from MPER domain of FIV gp36. The protein domain corresponding to the C8 sequence has

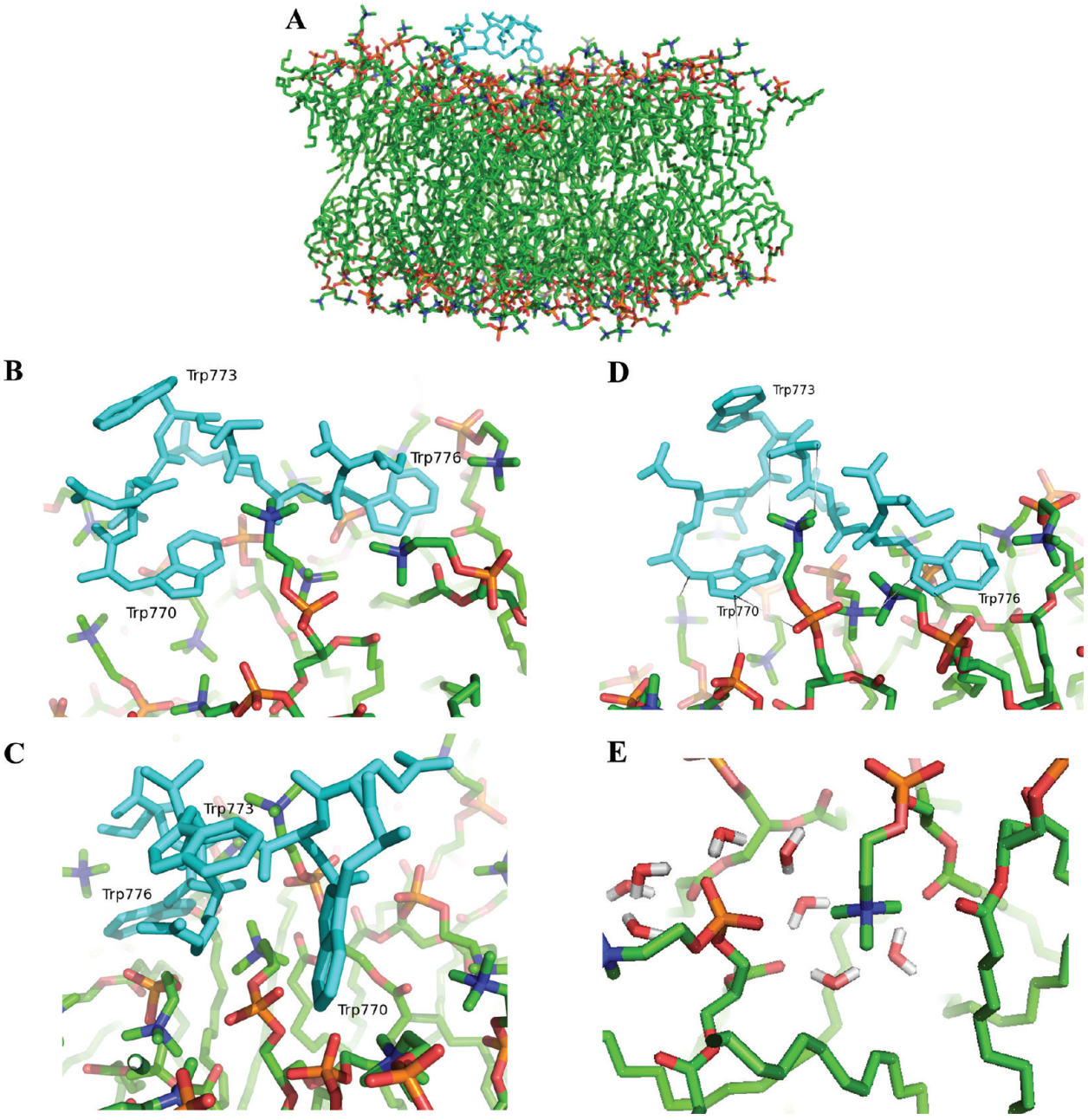

Figure 9. Configuration of the system when C8 has moved to the surface of the bilayer (panel A). Snapshots selected from the trajectories (panels B–D). C8 atoms are displayed in cyan, carbon atoms of POPC in green, oxygen atoms in red, nitrogen atoms in blue, and phosphorus in orange; water molecules are omitted. In panel D, hydrogen bonds and hydrophobic interactions are highlighted. In panel E, water molecules in the headgroup region of the leaflet in contact with the peptide are shown.

been hypothesized to exert a destabilizing effect on the target-cell membrane, favoring its fusion with the viral envelope. The presence of three Trp residues and their spatial arrangement has been found to be essential to promote the C8 interaction with lipid membranes.[15] However, to date the experimental approaches used do not have the necessary resolution to determine the atomic details of the interaction between the peptide and the lipids, and consequently the mechanism through which the peptide originates lipid bilayer perturbation remains unknown. In this work, we investigate the C8–POPC interactions combining a variety of experimental techniques with MD simulations. In particular, in our computations both the peptide and the lipids are considered at the atomistic level, thus allowing to analyze not only changes in peptide conformation but also perturbations in lipid packing due to peptide–bilayer interaction.

Concerning experimental data, we use the following: (i) neutron reflectivity to analyze peptide positioning relative to the bilayer as well as changes in the bilayer thickness upon peptide binding; (ii) CD to explore changes in C8 conformational preferences; (iii) spectrofluorimetry to highlight the polarity of the microenvironment experienced by the Trp residues and to estimate of the stoichiometry of the peptide–lipid interaction; and (iv) ESR spectroscopy to detect perturbations in lipid structuring and dynamics. The combined analysis

dx.doi.org/10.1021/jp204781a |*J. Phys. Chem. B* 2012, 116, 401–412

Table 3. POPC Bilayer Thickness

	POPC molecules, starting conformation	POPC molecules in contact with C8 before the binding	POPC molecules in contact with C8 upon the binding
P−P thickness (nm)	4.12[a]	4.00−4.03 (±0.02)	3.60−3.71 (±0.03)

[a] The value of bilayer thickness in the absence of the peptide, measured as the average distance between the phosphorus atoms of the upper and lower leaflets of POPC, is in agreement with previous computational[73] and experimental[74] studies.

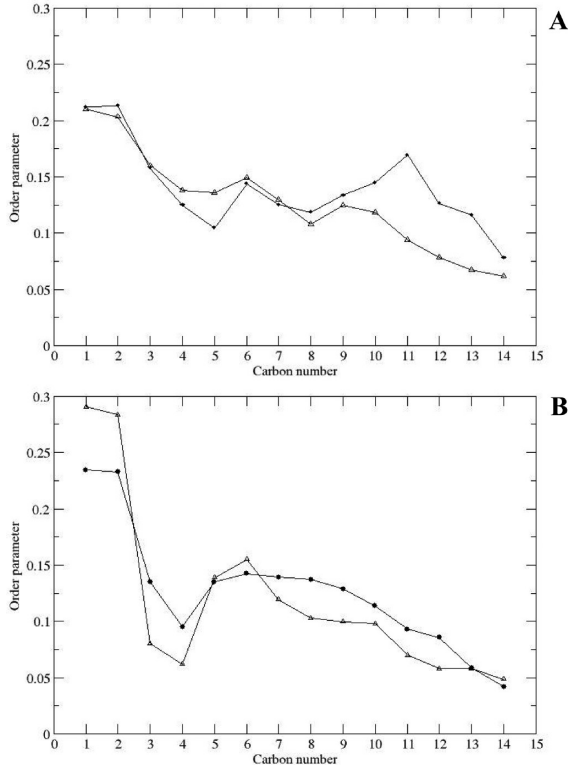

Figure 10. Calculated order parameters for POPC palmitic chains in direct contact with C8 (circles) and for those not in contact with the peptide (triangles) (panel A). Calculated order parameters for POPC palmitic chains of the leaflet in direct contact with the peptide (circles) and for those of the opposite side of the bilayer (triangles) (panel B).

of the results obtained by the different experimental techniques and MD data allows to obtain a complete description of the system structure and behavior at the molecular level. With respect to the reliability of the computational results, the limitations of our approach, of the force field, and of the limited time scales that can be sampled with current computer resources have to be recognized. One additional limitation of MD simulations is the small size of the membrane patch accessible to MD simulations.[60,61] In respect to the last point, it is known that the finite size of the simulation cell can influence the results, since the long wavelength undulations present in real membranes are suppressed by the PBCs employed in simulations, and that this suppression is manifested as a nonzero value of the surface tension.[62] Despite these and other restrictions, the results obtained by the simulations, which allow to capture the molecular details of the C8 binding to the membrane, are valuable, since this type of data is very difficult to be accessed from experiments.

Our data indicate that the C8 peptide adsorbs on the POPC bilayer surface positioning at 2−2.5 nm from the bilayer center, as suggested by both NR ρ profiles (see Figure 2) and MD density profiles (Figure 8). In particular, MD simulations show that the three C8 Trp residues are important in directing and anchoring the peptide to the membrane interface. In the literature, the role of Trp residues in proteins and peptides that interact with membranes is controversial. Some authors suggest that these residues have a role in aligning the proteins and peptides at the membrane−water interface;[63,64] others suggest that the Trp residues stabilize self-assembly of protein transmembrane domains deeply buried into the hydrophobic core of the membrane.[65] In our case, fluorescence spectra indicate that Trp residues remain exposed to the external aqueous medium. On the bases of these data, it can be speculated that the Trp ability to form hydrogen bonds with the POPC headgroup (Figure 9B−D), detected by our MD simulations, targets this residue to interfacial region between water and the hydrophobic core of the bilayer, thus hampering a deep insertion of C8 into the POPC membrane. Previous studies suggest that indoles are roughly aligned with the nearby lipids[17] or, alternatively, that the indole long axes are ∼60−65° from the membrane normal and the indole planes are at an oblique angle.[66] We do not find a preferential orientation of the indole plane with respect to the membrane bilayer. However, in this respect it should be recognized that our data could be affected by the use of a force field that does not exactly reproduce the Trp water−lipid bilayer partitioning.[67,68]

Upon membrane binding, C8 tends to assume a turn−helical conformation. Because of the short peptide sequence, the secondary structure dynamically changes with time. Nevertheless, both CD data and MD simulations show that an average of 2−4 residues are in this conformation. In a previous study in which several analogues of the C8 peptide have been considered, we have demonstrated that, once helically arranged, the WX_2WX_2W motif engenders a common orientation of the Trp residues on one side of the peptide, allowing a synergy among them in stabilizing the peptide−membrane interaction. Thus, our results indicate a strict interplay between peptide conformation and its membrane-interacting ability.[15,69]

A C8 molecule interacts with an average of 6−10 lipids simultaneously. This is shown by both fluorescence and MD data. However, simulations point out that a total of 24−30 different POPC molecules come in contact with the peptide. The peptide affects lipids order and dynamics. The peptide effect propagates along the lipid acyl chain until the deep interior of the bilayer. In particular, both the ESR and MD data clearly show that the presence of the peptide induces a reduction of the segmental acyl chain mobility for $n \geq 5-8$. These results are in agreement with those obtained by NR experiments showing, in the presence of the peptide, a change in the ρ value of the POPC acyl chain region. NR results also indicate that peptide binding increases the water content in the lipid headgroups region of the bilayer. These water molecules are involved in networks of H-bonds with the oxygen atoms of glycerol and choline groups and hydrate carbon atoms of the lipid headgroups, as highlighted by MD.

As a result of the peptide adsorption, a local reduction of the bilayer thickness by 2−5 Å is detected by both NR and MD results. In order to have a direct comparison between NR and computational results, the experimental scattering length density

profile, $\rho(z)$, of the two analyzed systems, using thickness values obtained by MD simulations, has been calculated (Figure S8 in the Supporting Information). The results of this analysis confirm a close correlation between NR and MD data. In more detail, MD results specify that the peptide adsorption perturbs the lipid packing and mobility in the bilayer leaflet in direct contact with the peptide, the opposite one being less perturbed. This marked asymmetry of the bilayer originates a sort of invagination, as well detectable in the MD simulation shown in Figure 9A. Thus, our results definitely highlight that changes in the POPC microstructuring due to the C8 interaction reflect on the lipid bilayer mesostructure.

5. CONCLUSIONS

The experimental strategy set up for this study has proved to be extremely informative of the microstructure and dynamics of complex systems such as lipid membranes interacting with peptides/proteins. Particularly, MD simulations have been found to be a valuable tool to rationalize all the experimental results obtained by neutron reflectivity, CD, EPR, and fluorescence spectroscopy. The findings of the present work could help in shedding light on the mechanism through which viral glycoproteins help to overcome the energetic barrier inherent with the fusion between the target cell plasma membrane and the viral envelope, and particularly on the role played by the MPER protein domain in the process. Our data suggest that lipid bilayer destabilization could be a consequence of the asymmetric perturbation of the bilayer that starts with an increased hydration of lipid headgroups coupled to an increase of lipid ordering in the leaflet exposed to the approaching viral glycoprotein. Headgroup hydration is fundamental in determining interfacial curvature of amphiphiles' aggregates.[70] In particular, since water organization at the membrane interface has been proposed to control the fusion dynamics,[71] the increment of bilayer hydration could be a fundamental part of role played by the MPER fusion protein domain during the process.

■ ASSOCIATED CONTENT

Supporting Information. Simulations of ESR spectra of 5-PCSL and 14-PCSL in POPC bilayers in the absence and in the presence of C8 peptide. Evolution of intermolecular distance and C8 conformation during MD simulations. NR and computational scattering length density profile, $\rho(z)$, of the POPC bilayer in the absence and in the presence of C8 peptide. This material is available free of charge via the Internet at http://pubs.acs.org.

■ AUTHOR INFORMATION

Corresponding Author

*E-mail: gerardino.derrico@unina.it. Phone: +39081674248. Fax: +39081674090.

■ ACKNOWLEDGMENT

The authors thank MIUR (PRIN 2008, grant no. 2006030935) for financial support and the Institut Laue-Langevin for awarding beam time.

■ REFERENCES

(1) Wickner, W.; Schekman, R. *Nat. Struct. Mol. Biol.* **2008**, *15*, 658–664.
(2) Harrison, S. C. *Nat. Struct. Mol. Biol.* **2008**, *15*, 690–698.
(3) White, J. M.; Delos, S. E.; Brecher, M.; Schornberg, K. *Crit. Rev. Biochem. Mol. Biol.* **2008**, *43*, 189–219.
(4) Chernomordik, L. V.; M.Kozlov, M. *Nat. Struct. Mol. Biol.* **2008**, *15*, 675–683.
(5) Lorizate, M.; Huarte, N.; Saez-Cirion, A.; Nieva, J. L. *Biochim. Biophys. Acta* **2008**, *1778*, 1624–1639.
(6) Pancino, G.; Camoin, L.; Sonigo, P. *J. Virol.* **1995**, *69* 2110–2118.
(7) Serres, P. F. *C. R. Acad. Sci. III* **2000**, *323*, 1019–1029.
(8) Frey, S. C.; Hoover, E. A.; Mullins, J. I. *J. Virol.* **2001**, *75*, 5433–5440.
(9) Giannecchini, S.; Bonci, F.; Pistello, M.; Matteucci, D.; Sichi, O.; Rovero, P.; Bendinelli, M. *Virology* **2004**, *320*, 156–166.
(10) Barbato, G.; Bianchi, E.; Ingallinella, P.; Hurni, W. H.; Miller, M. D.; Ciliberto, G.; Cortese, R.; Bazzo, R.; Shiver, J. W.; Pessi, A. *J. Mol. Biol.* **2003**, *330*, 1101–1115.
(11) Suarez, T.; Nir, S.; Goni, F. M.; Saez-Cirion, A.; Nieva, J. L. *FEBS Lett.* **2000**, *477*, 145–149.
(12) Salzwedel, K.; West, J. T.; Hunter, E. *J. Virol.* **1999**, *73*, 2469–2480.
(13) D'Errico, G.; D'Ursi, A. M.; Marsh, D. *Biochemistry* **2008**, *47*, 5317–5327.
(14) Giannecchini, S.; D'Ursi, A. M.; Esposito, C.; Scrima, M.; Zabogli, E.; Freer, G.; Rovero, P.; Bendinelli, M. *Clin. Vaccine Immunol.* **2007**, *14*, 944–951.
(15) D'Errico, G.; Vitiello, G.; D'Ursi, A. M.; Marsh, D. *Eur. Biophys. J.* **2009**, *38*, 873–882.
(16) Mitchell, T. W.; Ekroos, K.; Blanksby, S. J.; Hulbert, A. J.; Else, P. L. *J. Exp. Biol.* **2007**, *210*, 3440–3450.
(17) Grossfield, A.; Woolf, T. B. *Langmuir* **2002**, *18*, 198–210.
(18) Cordomi', A.; Perez, J. J. *J. Phys. Chem. B* **2007**, *111*, 7052–7063.
(19) Merlino, A.; Varriale, S.; Coscia, M. R.; Mazzarella, L.; Oreste, U. *J. Mol. Graph. Model* **2008**, *27*, 401–407.
(20) Varriale, S.; Merlino, A.; Coscia, M. R.; Mazzarella, L.; Oreste, U. *Mol. Phylogenet. Evol.* **2010**, *57*, 1238–1244.
(21) Anezo, C.; deVries, A. H.; Holtje, H. D.; Tieleman, D. P.; Marrink, S. J. *J. Phys. Chem. B.* **2003**, *107*, 9424–9433.
(22) Kandt, C.; Mátyus, E.; Tieleman, D. P. *Structure & Dynamics of Membranous Interfaces*; CRC Press, Taylor and Francis Group: Boca Raton, FL, 2007.
(23) Mátyus, E.; Kandt, C.; Tieleman, D. P. *Curr. Med. Chem.* **2007**, *14*, 2789–2798.
(24) Marsh, D.; Watts, A. *Lipid-Protein Interactions*; Jost, P. C., Griffith, O. H., Eds.;Wiley Interscience: New York, 1982; Vol. 2, pp 53−126.
(25) Marsh, D. *Curr. Opin. Colloid Interface Sci.* **1997**, *2*, 4–14.
(26) Wacklin, H. P.; Thomas, R. K. *Langmuir* **2007**, *23*, 7644–7651.
(27) Kaiser, E.; Colescott, R. L.; Bossinger, C. D.; Cook, P. I. *Anal. Biochem.* **1970**, *34*, 595–598.
(28) van der Wel, P. C. A.; Reed, N. D.; Greathouse, D. V.; Koeppe, R. E. *Biochemistry* **2007**, *46*, 7514–7524.
(29) Koeppe, R. E.; Sun, H.; van der Wel, P. C. A.; Scherer, E. M.; Pulay, P.; Greathouse, D. V. *J. Am. Chem. Soc.* **2003**, *125*, 12268–12276.
(30) Koenig, B. W.; Kruger, S.; Orts, W. J.; Majkrzak, C. F.; Berk, N. F.; Silverton, J. V.; Gawrisch, K. *Langmuir* **1996**, *12*, 1343–1350.
(31) Cubitt, R.; Fragneto, G. *Appl. Phys. A (Suppl.)* **2004**, *74*, S329–S331.
(32) Higgins, J. S.; Benoitt, H. C. *Polymers and Neutron Scattering*; Clarendon Press: Oxford, UK, 1994.
(33) Fragneto, G.; Thomas, R. K.; Rennie, A. R.; Penfold, J. *Langmuir* **1996**, *12*, 6036–6043.
(34) Thirtle, P. N. *Afit simulation program, v. 3.1*; Oxford University: Oxford, UK, 1997.
(35) D'Errico, G.; Vitiello, G.; Ortona, O.; Tedeschi, A.; Ramunno, A.; D'Ursi, A. M. *Biochim. Biophys. Acta* **2008**, *1778*, 2710–2716.
(36) Schorn, K.; Marsh, D. *Spectrochim. Acta A* **1997**, *53*, 2235–2240.

(37) Moro, G.; Freed, J. H. *J. Chem. Phys.* **1981**, *74*, 3757–3764.
(38) Della Lunga, G.; Pogni, R.; Basosi, R. *J. Phys. Chem.* **1994**, *98*, 3937–3942.
(39) Della Lunga, G.; Pezzato, M.; Baratto, M. C.; Pogni, R.; Basosi, R. *J. Magn. Reson.* **2003**, *164*, 71–77.
(40) Kelly, S. M.; Jess, T. J.; Price, N. C. *Biochim. Biophys. Acta* **2005**, *1751*, 119–139.
(41) Chakrabartty, A.; Kortemme, T.; Baldwin, R. L. *Protein Sci.* **1994**, *3*, 843–852.
(42) Christiaens, B.; Symoens, S.; Vanderheyden, S.; Engelborghs, Y.; Joliot, A.; Prochiantz, A.; Vandekerckhove, J.; Rosseneu, M.; Vanloo, B. *Eur. J. Biochem.* **2002**, *269*, 2918–2926.
(43) Lindahl, E.; Hess, B.; van der Spoel, D. *J. Mol. Model.* **2001**, *7*, 306–317.
(44) Giannecchini, S.; Di Fenza, A.; D'Ursi, A. M.; Matteucci, D.; Rovero, P.; Bendinelli, M. *J. Virol.* **2003**, *77*, 3724–3733.
(45) Merlino, A.; Vitagliano, L.; Ceruso, M. A.; Di Nola, A.; Mazzarella, L. *Biopolymers* **2002**, *65*, 274–283.
(46) Merlino, A.; Ceruso, M. A.; Vitagliano, L.; Mazzarella, L. *Biophys. J.* **2005**, *88*, 2003–2012.
(47) Merlino, A.; Esposito, L.; Vitagliano, L. *Proteins* **2006**, *63*, 918–927.
(48) Berendsen, H. J. C.; Postma, J. P. M; van Gusteren, W. F.; Di Nola, A.; Haak, J. R. *J. Chem. Phys.* **1984**, *81*, 3684–3690.
(49) Hess, B.; Bekker, H.; Berendsen, H. J. C.; Fraaije, J. G. E. M. *J. Comput. Chem.* **1997**, *18*, 1463–1472.
(50) Darden, T.; York, D.; Pedersen, L. *J. Chem. Phys.* **1993**, *98*, 1008–10092.
(51) Kabsch, W.; Sander, C. *Biopolymers* **1983**, *22*, 2577–2637.
(52) Vacklin, H. P.; Tiberg, F.; Fragneto, G.; Thomas, R. K. *Biochemistry* **2005**, *44*, 2811–2821.
(53) Galdiero, S.; Falanga, A.; Vitiello, G.; Vitiello, M.; Pedone, C.; D'Errico, G.; Galdiero, M. *Biochim. Biophys. Acta* **2010**, *1798*, 579–591.
(54) Spadaccini, R.; D'Errico, G.; D'Alessio, V.; Notomista, E.; Bianchi, A.; Merola, M.; Picone, D. *Biochim. Biophys. Acta* **2010**, *1798*, 344–353.
(55) Curtain, A.; Separovic, F.; Nielsen, K.; Craik, D.; Zhong, Y.; Kirkpatrick, A. *Eur. Biophys. J.* **1999**, *28*, 427–436.
(56) Gordon, L. M.; Curtain, C. C.; Zhong, Y. C.; Kirkpatrick, A.; Mobley, P. W.; Waring, A. J. *Biochim. Biophys. Acta* **1992**, *1139*, 257–274.
(57) Marsh, D. *Eur. Biophys. J.* **2010**, *39*, 513–525.
(58) Ambrosone, L.; D'Errico, G.; Ragone, R. *Spectrochim. Acta* **1997**, *53*, 1615–1620.
(59) Yoda, T.; Sugita, Y.; Okamoto, Y. *Chem. Phys. Lett.* **2004**, *386*, 460–467.
(60) Khandelia, H.; Ipsen, J. H.; Mouritsen, O. G. *Biochim. Biophys. Acta* **2008**, *1778*, 1528–1536.
(61) Feller, S. E. *Curr. Opin. Colloid Interface Sci.* **2000**, *5*, 217–223.
(62) Tobias, D.; Kechuan, T.; Klein, M. L. *Curr. Opin. Colloid Interface Sci.* **1997**, *2*, 15–26.
(63) Yau, W. C.; Wimley, W. C.; Gawrisch, K.; White, S. H. *Biochemistry* **1998**, *37*, 14713–14718.
(64) Mishra, V. K.; Palgunachari, M. N.; Segrest, J. P.; Anantharamaiah, G. M. *J. Biol. Chem.* **1994**, *269*, 7185–7191.
(65) Sal-Man, N.; Gerber, D.; Bloch, I.; Shai, Y. *J. Biol. Chem.* **2007**, *282*, 19753–19761.
(66) Esbjörner, E. K.; Caesar, C. E. B.; Albinsson, N.; Lincoln, P.; Nordén, B. *Biochem. Biophys. Res. Commun.* **2007**, *361*, 645–650.
(67) Villa, A.; Mark, A. *J. Comput. Chem.* **2002**, *23*, 548–553.
(68) Maccallum, J. L.; Tieleman, P. *J. Comput. Chem.* **2003**, *24*, 1930–1935.
(69) Scherer, E. M.; Leaman, D. P.; Zwick, M. B.; McMichael, A. J.; Burton, D. R. *Proc. Natl. Acad. Sci. U.S.A.* **2010**, *107*, 1529–1534.
(70) Costantino, L.; D'Errico, G.; Roscigno, P.; Vitagliano, V. *J. Phys. Chem. B* **2000**, *104*, 7326–7333.
(71) Peter, P. M.; Lindhal, E.; Pande, V. S. *J. Am. Chem. Soc.* **2011**, *133*, 3812–3815.
(72) Zamyatin, A. A. *Prog. Biophys. Mol. Biol.* **1972**, *24*, 107–123.
(73) Vaccaro, L.; Cross, K. J.; Kleinjung, J.; Strauss, S. K.; Thomas, D. J.; Wharton, A. S.; Skehel, J. J.; Fraternali, F. *Biophys. J.* **2005**, *88*, 25–36.
(74) Kinoshita, K.; Furuike, S.; Yamazaki, M. *Biophys. Chem.* **1998**, *74*, 237–249.